Proceedings of the 21st ICSMGE, Vienna, Austria, 14 – 19 June 2026. Pistrol, Adam & Schweiger (eds.)
Published by: ÖGG, Austrian Society for Geomechanics, Salzburg, Austria, ISBN 978-3-9503898-4-5
https://doi.org/10.53243/ICSMGE2026-997

Assessment of vegetated slope instability using field hydraulic and electrical data

Ruimin Chen, Wei Wu
Institute of Geotechnics, BOKU University, Vienna, Austria, wei.wu@boku.ac.at

Wenbin Jian
Zijin School of Geology and Mining, Fuzhou University, China

ABSTRACT: In-situ monitoring is essential for slope stability analysis, offering real-time hydro-mechanical data for accurate slope behavior characterization. Recently, a slope assessment framework using electrical data has proven effective. However, vegetation roots widely distributed in shallow unsaturated slopes influence soil hydrology and stability, while seasonal variations modulate their effects on both hydraulic and electrical properties. Therefore, further research is required to adapt the assessment framework for vegetated slopes. The in-situ volumetric water content, matric suction, and electrical conductivity were monitored at a vegetated shallow landslide site in southeast China. The relationship between electrical conductivity and volumetric water content across seasonal variations was investigated. Then, models for matric suction, suction stress, and shear strength of unsaturated soil were extended by associating them with electrical conductivity. Specifically, the root-induced shear strength increment was derived considering the Wu model, with root tensile strength and root area ratio obtained through laboratory experiments and field observations, respectively. To validate this framework, the hydro-mechanical-electrical coupling problem was simulated using COMSOL Multiphysics, where slope instability induced by rainfall was estimated based on the local safety factor. The simulated electrical conductivity and displacements showed good agreement with the monitored data. Moreover, the trend of calculated local safety factor was consistent with the shear strength derived using electrical conductivity as a variable. The results demonstrate that the hydraulic processes in vegetated unsaturated slopes and their instability can be reasonably evaluated by the proposed framework. This work extends the application of electrical data to assess the properties of vegetated soil and improves the understanding of the mechanisms of landslide hazards.

KEYWORDS: Field monitoring data, unsaturated soil mechanics, electric conductivity, vegetated slope stability, numerical modeling.

1 INTRODUCTION

Extreme rainfall events have become more frequent and intense in recent decades due to climate change, increasing the risk of rainfall-induced landslides. Such landslides are often sudden, widespread, and highly destructive. Heavy rainfall raises soil water content and pore pressure, reducing matric suction and shear strength, thereby increasing the likelihood of slope failure (Świtała and Wu, 2018). On vegetated slopes, root systems further complicate this process by altering water flow and reinforcing the soil, directly affecting slope stability. Therefore, understanding root-soil interactions is essential for evaluating the behavior of rooted landslides.

Long-term in-situ monitoring generates extensive data on hydrological and mechanical processes, providing critical insights into slope behavior. Recent studies have combined field monitoring with geophysical techniques, such as electrical resistivity tomography and other conductivity-based methods, to explore soil properties. Notably, a framework linking shear strength to electrical conductivity was proposed and later extended to relate conductivity to suction stress and matric suction (Crawford and Bryson, 2018; Crawford et al., 2019). However, few studies have addressed seasonal changes in root activity and their effect on hydro-electrical interactions under long-term monitoring (Ni et al., 2019).

In this study, in-situ measurements of volumetric water content, matric suction, and electrical conductivity were conducted at a vegetated shallow landslide site in southeast China. Seasonal variations in the relationship between soil moisture and electrical conductivity were examined. Based on the observations, models for matric suction, suction stress, and shear strength were extended to incorporate electrical conductivity in rooted soils. Coupled hydro-mechanical-electrical simulations using COMSOL Multiphysics were carried out to evaluate slope stability. The results highlight the value of electrical data in characterizing root-influenced soil behavior and improving understanding of rainfall-induced landslides.

2 SITE DESCRIPTION

2.1 *Geological condition and soil properties*

The monitored landslide is situated in Sanming City, Fujian Province, China. The region lies within a subtropical maritime monsoon climate zone. It receives abundant rainfall, largely driven by the southeast monsoon.

The monthly average precipitation at the Sanming Sanyuan Meteorological Station (Station ID: 58828; coordinates: 117°37′12″ E, 26°16′12″ N) from 2017 to 2024 is illustrated in Figure 1. It presents a box-violin plot of monthly precipitation, which reveals a clear seasonal pattern: rainfall is predominantly concentrated between May and August. During this period, the average precipitation is significantly higher than in other months, accounting for approximately 52% of the total annual rainfall.

The study area mainly consists of low to medium mountains and hilly terrain. Geologically, it belongs to the regional unit of Gneissic Biotite Monzogranite. This formation is part of the First Intrusive Phase from the Early Yanshanian Period.

The investigated landslide is an old, shallow-type feature located at elevations ranging from 830 to 860 m. The slope has a general orientation of 275°. Its dimensions are approximately 40 m wide and 50 m long.

A humus and root layer, approximately 0.5 m thick, covers the surface of the landslide. Beneath this lies granitic residual soil with a depth of 0.3–2.1 m, classified as Thermic Typic Kandiudults and exhibiting a clay loam texture. The upper part of the slope consists of sandy decomposed granite, while the lower part is made up of completely weathered granite with a fragmented structure. Moderately weathered granite bedrock appears at greater depths.

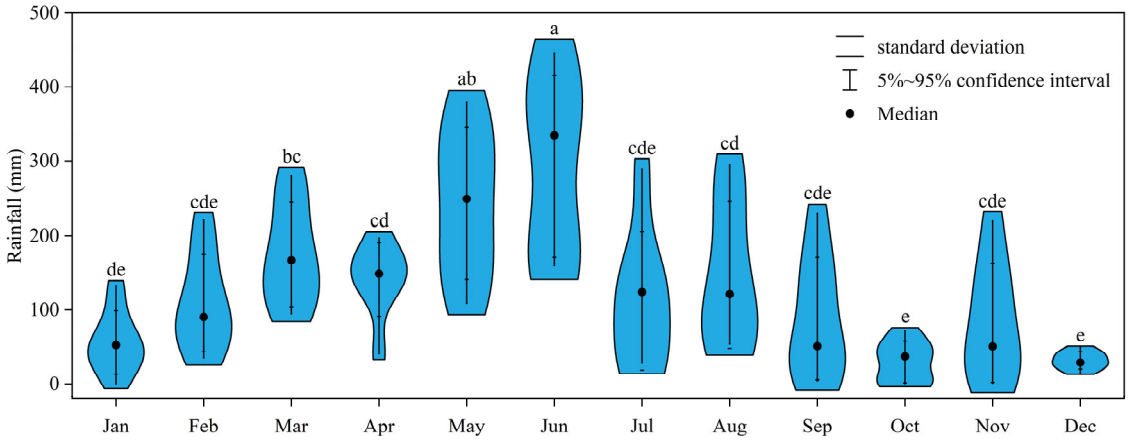

Figure 1. Box violin plot of monthly average rainfall.

2.2 *Field monitoring instrumentation*

Two field monitoring stations were installed, as shown in Figure 2. They recorded changes in the vegetated landslide, including rainfall, electrical conductivity, temperature, soil water content, matric suction, and displacement. Sensors were installed vertically at depths of 50, 100, 150, and 200 cm. Data were collected every 30 minutes and uploaded to a cloud server. The dataset used in this study covers the period from January 21, 2021, to September 13, 2023, totaling 814 days. Before installation, each instrument was calibrated in the lab using undisturbed soil from the site.

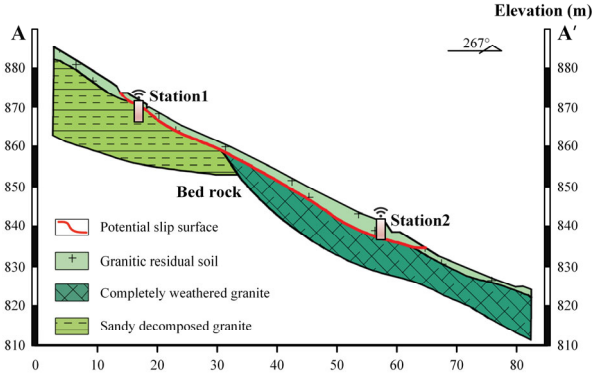

Figure 2. Schematic diagram of the geological cross-section.

3 FIELD HYDRAULIC AND ELECTRICAL DATA

Total rainfall over the monitoring period was around 3700 mm. Annual totals were generally lower than the historical average of 1700 mm per year.

3.1 *Field-measured volumetric water content*

Field data indicate that volumetric water content followed a consistent pattern across depths, with smaller fluctuations at greater depths. At Station 1, between September 1 and December 13, 2021, water content at 50 cm declined from 43.81% to 30.73%, while at 200 cm it dropped from 41.12% to 35.56%. The fluctuation at 50 cm exceeded that at 200 cm by 7.52%. At Station 2, the difference was 6.45%. This can be explained by higher density and lower void ratio in deeper soils, which reduce pore space and help retain water. In general, deeper layers held more moisture. At Station 2, the average content at 50, 100, 150, and 200 cm was 37.49%, 38.64%, 42.53%, and 43.34%, respectively.

3.2 *Field long-term soil-water characteristic curves*

Matric suction reflects the water retention behavior of partially saturated soils and generally decreases as water content increases. Based on long-term field monitoring data, the observation period can be roughly divided into two stages: drying or wetting. For each stage, the soil-water characteristic curve (SWCC) can be fitted using the van Genuchten model (van Genuchten, 1980), which describes the relationship between volumetric water content and matric suction:

$$\theta = \theta_r + \frac{(\theta_s - \theta_r)}{\{1 + [u_a - u_w]^n\}^m} \quad (1)$$

where $(u_a - u_w)$ is the matric suction of soil (kPa), u_a is the pore-air pressure (kPa), u_w is the pore-water pressure (kPa), θ is the volumetric water content (%), θ_r and θ_s are the residual and saturated water content of the soil (%), respectively. In this study, the fitting parameters α and n were obtained from the data, with m set to $1 - 1/n$.

The fitted van Genuchten parameters for Station 2 are summarized in Table 1. At the same location, drying and wetting paths show distinct parameters, likely due to seasonal shifts in soil moisture. This hysteresis may stem from the inkbottle effect, trapped air, and contact angle differences at the soil-water interface. As a result, the drying path typically exhibits higher water content at a given suction, yielding a higher air-entry value (AEV).

Table 1. Parameters of the van Genuchten model for Station 2.

Parameter at Station 2	Drying	Wetting
α	0.0895	0.2812
n	1.3854	1.3271
m	0.2782	0.2456
θ_r	0.1107	0.1084
θ_s	0.4847	0.4644
$AEV(kPa)$	4.57	1.47
R^2	0.7513	0.7442

The AEV indicates the suction point where desaturation starts, marking the onset of air-filled pores and reduced capillary forces. The AEV at Station 2 is slightly higher along the drying path, likely due to residual water films and stronger capillary forces in finer pores. These effects delay air entry, raising the suction threshold compared to the wetting path.

Hysteresis should also be considered in modeling unsaturated soil behavior. The coefficient of determination (R^2)

for all fitted SWCCs ranges around 0.75. During wetting periods, delayed infiltration causes uneven moisture and unsaturated zones, lowering water content and introducing outliers below the wetting curve. This reduces the fit quality, resulting in slightly lower R^2 values for the wetting path than for the drying path.

3.3 *Relationship between field hydraulic and electrical data*

Electrical conductivity varies with soil type, pore structure, and plant activity, even at the same moisture level. Since it also differs between hydraulic paths, an effective value is defined using a formula analogous to degree of saturation.

$$EC_e = \frac{EC - EC_r}{EC_s - EC_r} \tag{2}$$

where EC_e is the effective electrical conductivity, and EC_s and EC_r are the conductivities at saturated and residual water content, respectively.

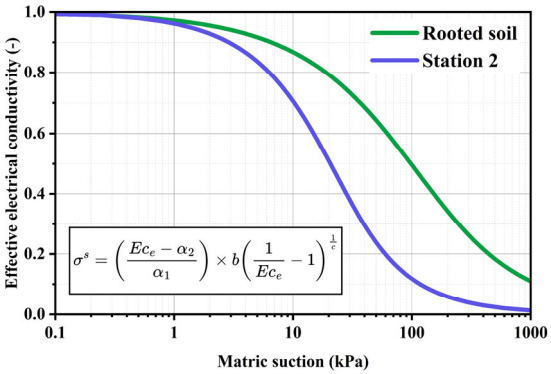

Figure 3. SSEC model for suction stress and electrical conductivity.

Figure 3 shows the relationship between degree of saturation and effective electrical conductivity during different hydrological periods, fitted using a linear equation:

$$EC_e = \alpha_1 S_e + \alpha_2 \tag{3}$$

where α_1 and α_2 are the slope and intercept. The results indicate a clear linear relationship between effective electrical conductivity and degree of saturation. Based on this, the soil–water potential-electrical conductivity (SWEC) model was proposed (Crawford and Bryson, 2018), in which conductivity is treated similarly to the SWCC. Based on the SWEC framework, suction stress can be expressed through effective conductivity, forming the suction stress-electrical conductivity (SSEC) curve (Figure 3).

3.4 *Shear strength*

Since suction stress has been related to electrical conductivity (see Figure 3), it can be incorporated into the shear strength equation by substituting the SWEC expression into the original formulation. It is expressed as:

$$\tau = c' + (\sigma - u_a)\tan\varphi' + \left[\left(\frac{EC_e - \alpha_2}{\alpha_1}\right) * b\left(\frac{1}{EC_e} - 1\right)^{\frac{1}{c}}\right]\tan\varphi' \tag{4}$$

where τ is the shear strength of soil, c' is the effective cohesion (the portion independent of net stress or suction), and $\sigma - u_a$ is the net normal stress, with σ as total normal stress. φ' denotes the internal friction angle under effective stress, b and c are fitting parameters of SWEC model. Other parameters are defined as previously described.

4 NUMERICAL MODEL

4.1 *Conceptual modeling of a vegetated slope*

The conceptual model of the vegetated slope is developed based on the A-A′ cross section (Figure 2). As shown in Figure 4, the slope consists of a 0.5 m surface layer of rooted soil, underlain by 1.5 m of unrooted soil, with weathered bedrock beneath. The model is discretized into triangular elements, comprising 5137 vertices and 9894 elements, including 805 boundary elements and 361 vertex elements. Mesh refinement is applied around rear-edge cracks and the slope toe to minimize numerical errors and ensure stability.

Table 2. Summary of input parameters for simulation.

Type	Parameter	Rooted soil	Unrooted soil
Hydraulic parameters	θ_s	0.4447	0.4644
	θ_r	0.1779	0.1084
	α	0.0255	0.2812
	n	1.2344	1.3271
	K_s	2.83E-4	2.05E-4
	ρ	1650	1750
Mechanical parameters	E	20	20
	υ	0.3	0.3
	c'	26.7	9.3
	φ'	32.6	32.6

Note: θ_s, θ_r, α, and m are parameters of the van Genuchten model for the field SWCC; K_s is the saturated permeability (cm/s). ρ is the porosity of the soil (kg/m^3), E denotes the Young's modulus (MPa), υ denotes the Poisson's ratio (-), c' denotes the cohesive intercept under effective stress (kPa), and φ' represents the internal friction angle under effective stress (°).

For hydrological boundaries, the top is defined as a rainfall boundary with intensity matching the field data and a ponding depth of 0.05 m. The right boundary is set as a drainage outlet, while the left and bottom boundaries are no-flux. For mechanical boundaries, the top surface is free, the bottom is fixed, and the two sides are constrained with roller boundaries to restrict horizontal movement.

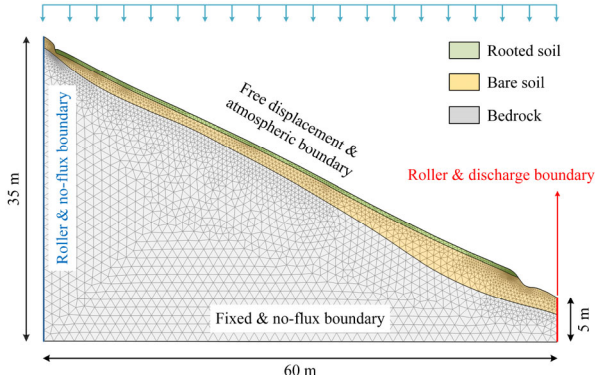

Figure 4. Conceptual model and boundary conditions.

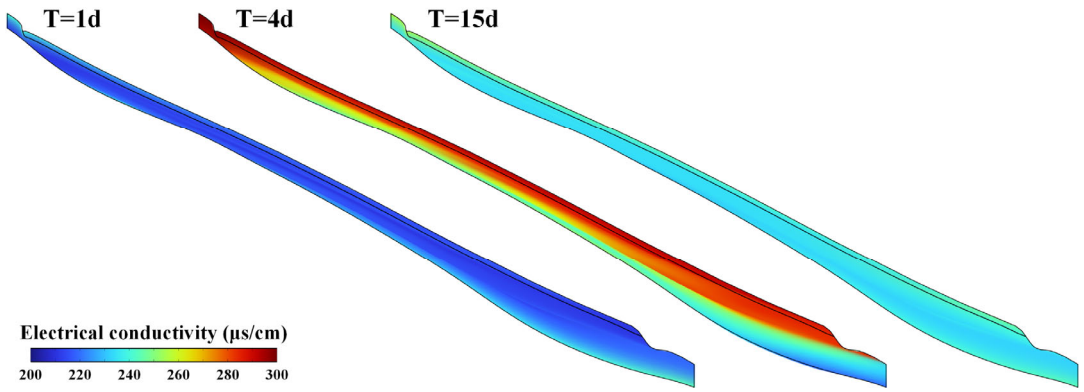

Figure 5. Time snapshots of the simulated electrical conductivity at *T*=1,4, and 15 d.

In this study, pore water pressure is used as the primary variable in the Richards equation, which is extended to describe saturated-unsaturated flow. Changes in electrical conductivity are driven by soil moisture variations, enabling hydro-electrical coupling. Different hydro-electrical relationships are applied to capture root effects on soil properties. For rooted soil, the parameters α_1 and α_2 are 1.30 and –0.34; for unrooted soil, they are 1.33 and –0.39. The outer boundary is set as insulating to ensure charge conservation.

4.2 *Analysis results*

The potential sliding zone was illustrated with a cloud map showing changes in EC (Figure 5). At T = 1 d, EC increases with depth and is relatively uniform. During intense rainfall (T = 4 d), EC rises sharply in the shallow rooted zone, forming a distinct wetting front with depth. By T = 15 d, the profile becomes stable, though EC remains higher in the rooted layer than in the unrooted layer. Simulated displacements at Station 2 agree well with monitored data (Table 3), especially at T = 15 d, when simulated and observed EC and displacement closely match. Overall, the trends are consistent.

Table 3. Comparison between simulated results and monitored data.

Data	Time	Monitored	Simulated
EC ($\mu s/cm$)	T=1 d	0.0895	0.2812
	T=4 d	1.3854	1.3271
	T=15 d	0.2782	0.2456
Displacement (mm)	T=1 d	0.1107	0.1084
	T=4 d	4.57	1.47
	T=15 d	0.7513	0.7442

The local factor of safety (LFS) was used to assess the evolution of unstable zones. In parallel, shear strength estimated from electrical conductivity was compared with LFS at the same depths (Table 4). The two measures show similar responses to stability changes after rainfall, and this relationship may be expressed by a linear equation. Therefore, electrical conductivity can be considered a reliable indicator for assessing slope stability in vegetated slopes.

$$\tau = 4.77LFS + 11.51 \quad (4)$$

Table 4. Comparison of LFS and shear strength at 200 cm depth, Station 2.

Time	LFS	Shear strength
T=1 d	4.78	35.42
T=4 d	0.94	16.81
T=15 d	2.03	17.93

5 CONCLUSIONS

In-situ monitoring at a vegetated shallow landslide site in southeast China revealed seasonal variations in the relationship between soil moisture and electrical conductivity. Electrical conductivity was effectively incorporated into models for matric suction, suction stress, and shear strength in rooted soils. Field-derived SWCCs for rooted and unrooted soils were complemented by SWEC and SSEC relationships from conductivity data. Coupled hydro-mechanical-electrical simulations reproduced observed displacements and safety factor trends, with simulated conductivity closely matching field measurements. These results demonstrate that electrical measurements reliably assess slope stability and root–soil interactions, and that the proposed conductivity-based framework is a practical tool for monitoring and early warning of rainfall-induced landslides.

6 ACKNOWLEDGEMENTS

The authors are grateful to the financial supports from National Natural Science Foundation of China (NSFC-CONICYT, U2005205; 41861134011), European Commission Horizon Europe Marie Skłodowska-Curie Actions Staff Exchanges Project-LOC3G (Grant No. 101129729), and OeAD WTZ Project (No. MULT 01/2023).

7 REFERENCES

Asadzadeh, M., and Soroush, A. 2017. Macro- and micromechanical evaluation of cyclic simple shear test by discrete element method. *Particuology* 31, 129-139.

Crawford, M.M. and Bryson, L.S., 2018. Assessment of active landslides using field electrical measurements. Engineering Geology, 233, pp.146–159.

Crawford, M.M., Bryson, L.S., Woolery, E.W. and Wang, Z., 2019. Long-term landslide mwonitoring using soil-water relationships and electrical data to estimate suction stress. Engineering Geology, 251, pp.146–157.

van Genuchten, M.Th., 1980. A Closed-form Equation for Predicting the Hydraulic Conductivity of Unsaturated Soils. Soil Science Society of America Journal, 44(5), pp.892–898.

Ni, J.-J., Cheng, Y.-F., Bordoloi, S., Bora, H., Wang, Q.-H., Ng, C.-W.-W. and Garg, A., 2019. Investigating plant root effects on soil electrical conductivity: An integrated field monitoring and statistical modelling approach. Earth Surface Processes and Landforms, 44(3), pp.825–839.

Świtała, B.M. and Wu, W., 2018. Numerical modelling of rainfall-induced instability of vegetated slopes. Géotechnique, 68(6), pp.481–491.